Ionospheric Channel Modeling and Estimation

by

Wylie Standage-Beier

A Thesis Presented in Partial Fulfillment
of the Requirement for the Degree
Master of Science

Approved November December 2017 by the
Graduate Supervisory Committee:

Daniel W. Bliss, Chair
Chaitali Chakrabarti
Thomas McGiffen

ARIZONA STATE UNIVERSITY

December 2017

ABSTRACT

The goal is to provide accurate measurement of the channel between a ground source and a receiving satellite. The effects of the the ionosphere for ground to space propagation for radio waves in the 3-30 MHz HF band is an unstudied subject. The effects of the ionosphere on radio propagation is a long studied subject, the primary focus has been ground to ground by means of ionospheric reflection and space to ground corrections of ionospheric distortions of GPS. Because of the plasma properties of the ionosphere there is a strong dependence on the frequency of use. GPS L1 1575.42 MHz and L2 1227.60 MHz are much less effected than the 3-30 MHz HF band used for skywave propagation. The channel between the ground transmitter and the satellite receiver is characterized by 2 unique polarization modes with respective delays and Dopplers. Accurate estimates of delay and Doppler are done using polynomial fit functions. The application of polarimetric separation of the two propagating polarizations allows improved estimate quality of delay and Doppler of the respective mode. These methods yield good channel models and an effective channel estimation method well suited for the ground to space propagation.

ACKNOWLEDGMENTS

I would like to acknowledge and thank my thesis adviser Dr. Daniel Bliss at Arizona State University School of Electrical, Computer and Energy Engineering for his guidance and support. His access was always available to challenge and guide my research. He encouraged me to create a document based on my research and my own words. Further he was available to direct my course of inquiry as needed and steer me to present in a clear manner.

I would also like to thank the menbers of my thesis committee, who included Dr. Chaitali Chakrabarti and Dr. Tom McGiffen .

I would also like to acknowledge and thank the scientists who have brought this field forward through the last century and provided a bedrock to start and continue by research.

I would also like to thank my technical reviewers Richard Gutierrez and the rest of the WISCA lab.

Finally, I would like to thank my parents for their complete confidence and support of my years of study culminating in my current research project and thesis.

Wylie Standage-Beier

TABLE OF CONTENTS

CHAPTER Page

CHAPTER Page

LIST OF FIGURES

LIST OF TABLES

Table Page

Chapter 1

INTRODUCTION

The main focus of this document is channel estimation and modeling of the trans-ionospheric ground to space High Frequency (HF) channel. Channel modeling and estimation for ground to ground communications in the HF band is a long studied subject. The large number of applications and large user base is the driving force behind the ground to ground study. This is not the case for the trans-ionospheric channel. Only a small number of applications currently use any information about the upper ionosphere. The Gobal Positioning System (GPS) and the GPS performance enhancement Wide Area Augmentation System (WAAS) both make use of Total Electron Count (TEC) measurements to correct for ionospheric distortion [1][2]. Because of the nature of the frequency of GPS signals being much higher in frequency, about 1.5 GHz versus 3-30 MHz of the HF band, they are much less effected by the structure of the ionosphere. Increasing application of HF for Over The Horizon Radar (OTHR), Over The Horizon Communications (OTHC), Geo-location, and many other HF based applications have given rise to the need for space based augmentation to systems and improved modeling [3]. This document focuses on the channel estimation and how the channel estimate feeds into a larger ionosphere modeling system.

1.1 Background

The ionosphere is a long studied subject because of the strong effect on early radio propagation. Quality of understanding needed for basic understanding of ground to ground is limited. The structure of the upper ionosphere has no effect on the propagation of ground to ground communications. Study of the upper ionosphere

was untouched until early in the space age with the ability to look down into the ionosphere from orbit. This difference of propagating paths can be seen in Figure 1.1 on page 3 showing the divide between ground to ground propagation and ground to space propagation. Using some of the methods when observing the ionosphere from the ground, space based observations did not provide a full picture of the ionosphere. Because of the nature of the measurement methodology, measurements of the close to the divide of bottom and top of the ionosphere are subject to lower fidelity. Until the advent of GPS there was no system affected by or could make use of this information about the upper ionosphere. The frequencies of operation of GPS is less sensitive to the effects of the ionosphere structure and only the total amount of electrons between the GPS satellites and the receiver.

1.1.1 Ionosphere

The ionosphere is the upper layer of the earths atmosphere characterized by higher charged particle density. Starting around 100 kilometers and extending past 1000 kilometers. This density of charged ions causes reflections and refractions of electromagnetic waves. These effects are frequency dependent and strongest effects are on the MF and HF frequency bands. The mechanism and effects of the ionosphere are discussed in greater detail in chapter 2. Figure 1.1 shows a cartoon depiction propagation from ground to space and ground to ground propagation.

1.1.2 History

The electrical properties of the ionosphere are a long studied subject. The aurora borealis, also known as the northern lights, is most likely the first observation of the ionosphere. The first trans-Atlantic radio transmission on December 12th 1901 by Guglielmo Marconi was only possible because of the ionosphere making this the first

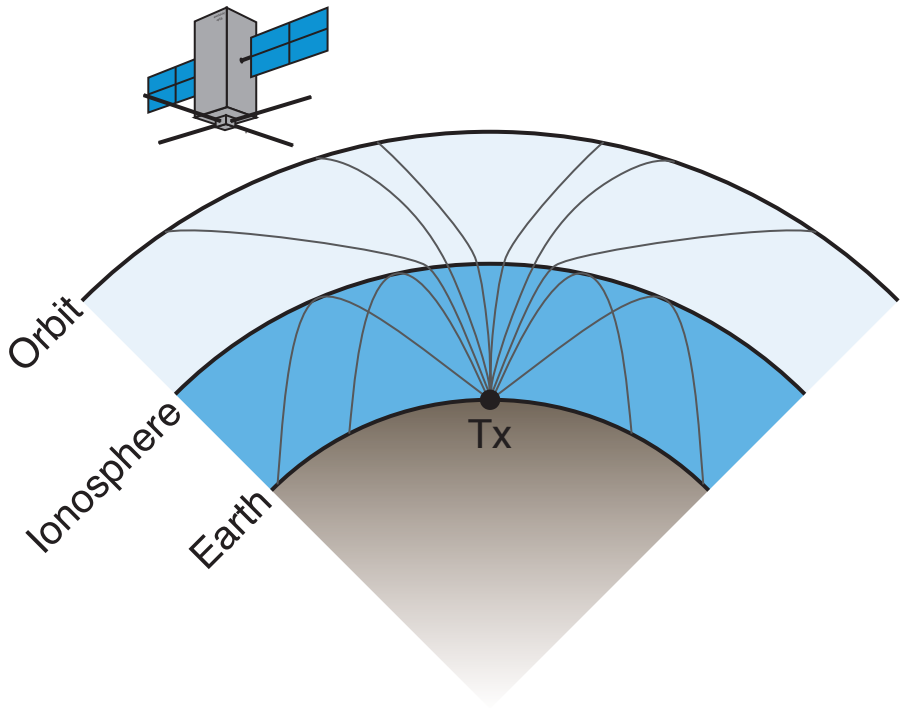

Figure 1.1: Diagram of Propagation Throw the Ionosphere

experiment directly involving the ionosphere in radio propagation. This, however, did not confirm the existence of the ionosphere. By 1914 two engineers, Leed de Forest and L.F. Fuller, working for the US Federal Telegraph Company came to the conclusion there where two paths of propagation with unique delays and amplitudes. The respective paths are surfaces waves and ionosphere bonce. Again this did not confirm the existence of the ionosphere. Because of advances in radio's higher frequency, power, and waveform more sophisticated measurements became possible. The 1920's and the advent of high frequency or shortwave radios made more sophisticated measurements possible. In 1927 Edward V. Appleton confirmed the existence of the ionosphere; he was awarded the Noble prize in physics 20 years later in 1947. The ad-

vent of radar direct measurements of ionosphere by means of ionosounders. Upward looking radars provide ionospheric reflectivity measurements vs altitude. This is the current method for measuring electron density profile of the ionosphere [3].

All the previously discussed advances only observe the bottom of the ionosphere or everything below the point where nothing is returned to the ground. Measurements of the ionosphere above the bottom where not practical until the advent of space craft and satellites. The upper structure of the ionosphere was a subject of early study in the space age. In 1962 a joint Canadian-American mission Alouette 1 launched a satellite equipped HF ionosounder. This was followed up Alouette 2 in 1965. NASA followed in 1972 and 1975 with AEROS A and B. These satellites provided measurements of the highest layers of the ionosphere. The 1970's and 80's brought the advent of GPS. Wide spread regular measurements of the ionosphere's total electron count became possible; however, because reasons discussed in Chapter 2 on page 7 little information about the structure of the ionosphere can be inferred [1][3][4][5]. This information is sufficient to improve GPS location performance. This information is used in the GPS enhancement called Wide Area Augmentation System (WAAS). The WAAS GPS system is currently finding use improving positional accuracy of everything from smart phones to self driving cars to aircraft and drones. Currently there is no regular measurement of the upper ionosphere. This paper focuses on the analysis of the problem of modeling propagation thought the ionosphere and the estimation of useful parameters formed measured data.

1.2 Literature Survey

The subject of ionospheric channel models is usually approached as ground to ground by single or multiple bounces off the ionosphere. This kind of problem has been studied for over one hundred years; however, this is not the problem of focus in

this document. Everything up to and including the upper most part of the ionosphere reachable in ground to ground propagation is the bottom side. The Top side is everything above the bottom side. Ground to space is the primary focus of this document and therefore the top and the bottom sides of the ionosphere have a strong influence on HF propagation. The bottom side of the ionosphere is regularly measured using ionosondes. These measurements are combined and averaged over a month to form the International Reference Ionosphere (IRI). The IRI model is a common starting place for most bottom side modes of the ionosphere. IRI is deficient in detail about the Top side of the ionosphere. The overwhelming amount of study in the area of the top side is with the focus of correction of GPS errors. Because the frequencies used by GPS, the effects of the ionosphere's structure are minimized. This is discussed in more detail in Chapter 2 Sections 2.2 and 2.3.2.

The International Reference Ionosphere is a monthly rolling average of the ionosphere structure as observed using ionosondes and total electron count measurements[6]. This averaging largely suppresses time and local variations. Multiple Assimilation based models claiming improvements correcting for this averaging have been proposed. [7][8][9][10][11]

GPS makes use of models and measurements of the ionosphere used for GPS correction ionospheric distortion causing position and timing errors. The Klobuchar model approximates the ionosphere as a single thin layer of elevated free electron density at an altitude of 350 KM [1]. Klobuchar model is not the most sophisticated model of the ionosphere used for GPS. NeQuick assumed electron density profiles verse altitude. The original version of NeQuick used Epstein layers as the models for different layers of the ionosphere scaled to match the observations[5]. Subsequent improvements to NeQuick have improved upon the use of Epstein layers as the basis to the model. NeQuick has been proposed as an inproved top side approximation for

the IRI model[12]. These corrections make use of regular GPS based total electron count. measurements the ionosphere.

1.3 Purpose of Work

The purpose of this work in to provide tools for providing an accurate measurement of the Ionosphere state and structure. While currently there is no existing source of information about the structure and ion density. This document focuses on the methods of modeling the ionosphere and using measured data to arrive at a meaningful estimate of the ionosphere. These measurements and techniques yield additional information about both the bottom and top half's of the ionosphere. Existing ground based methods only yield information about the ionosphere up to some altitude dividing the top from the bottom. This additional information about the top side makes correction of space based OTHR and geolocation possible with enhanced performance.

1.4 Overview

The intention of this document is to describe the problems, setup and methods applied to channel modeling and estimation. Chapters 1 and 2 describe background and setup to to the problem of ionosphere channel modeling and estimation. Chapter 3 goes into detail about the experimental and simulation setups. Methods applied to channel estimation are described in detail in chapter 4. Chapters 5 and 6 expand on the results of chapter 4 and describe future direction of work.

Chapter 2

IONOSPHERE STRUCTURE, PROPERTIES, AND MEASUREMENTS

The upper atmosphere of the earth is under very low pressure and exposure to ionizing radiation. This low particle density and high ionizing radiation flux causes longer ion recombination times and higher ion formation rate giving this region of the atmosphere the name of the ionosphere. These ions are a plasma of varying density primarily altitude however many other factors have strong effects. Time of day, solar activity, and many other factors that are beyond the scope of this document. This varying plasma density has varying propagation properties including speed and impedance. The changing impedance with position causes refraction and reflection of radio waves in the ionosphere. This refraction and reflection cause the path to deviate from the free space path. In addition to refractions and reflections the medium is depressive supporting 2 propagating polarizations. All of these effects are frequency dependent and will be discussed in Section 2.2 starting on page 11.

2.1 Ionosphere Structure

The Ionosphere is a structure is composed of layers of varying ion density. Ion density is the driving property effecting electromagnetic propagation. The ionosphere is composed of 3 primary layers D, E, and F that are each composed of sub layers. These layers and sub layers are not always well separated. These layers all exhibit some correlation to time of day and solar activity dependence. The D layer is the lowest layer at altitudes of 50 to 90 KM and is composed of no sub-layers. The primary ion source for the D layer is Nitrous Oxides ionized by hard X-ray radiation. The E layers is at 90 to 140 KM and are formed by soft X-ray radiation ionizing molecular

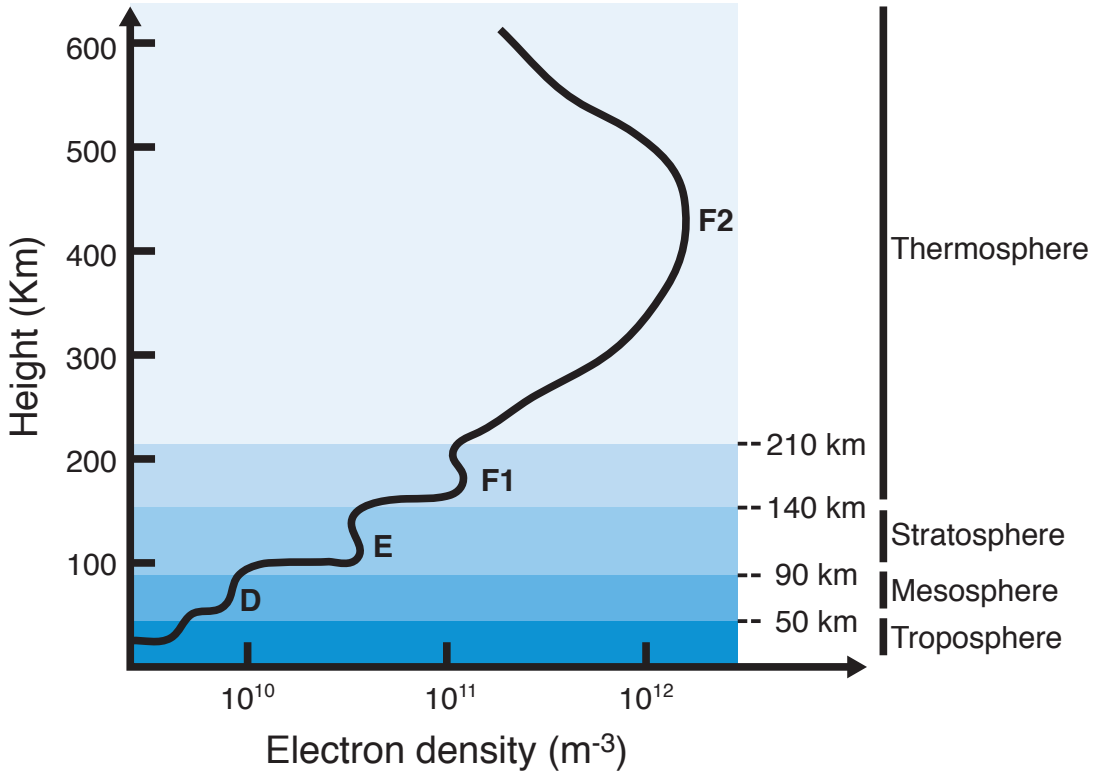

Figure 2.1: Day Time Ionosphere of Atmosphere

oxygen at altitudes from 90 to 140 KM. The F layers are the highest altitude and most dense layers of the ionosphere. Some of this structure can be seen in Figure 2.1 on page 8. Above the F layers is the top side of the ionosphere. Top side is progressive decreasing density of electrons, however little information exists about structure of the ionosphere.

2.1.1 Day and Night

The primary time dependence of the ionosphere is the solar day. This is most apparent in the D layer in the day and it's disappearance at night. The D layer

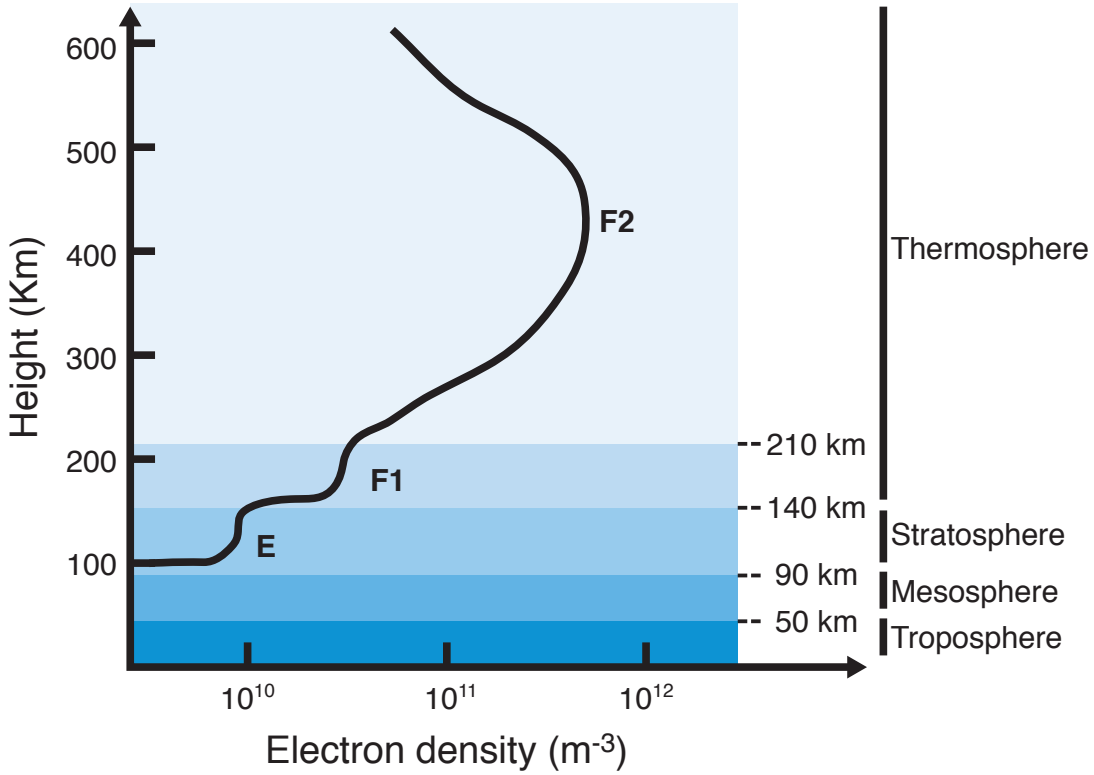

Figure 2.2: Night Time Ionosphere of Atmosphere

accounts for the shorter range of ionosphere bound ground to ground communications during the day. Figure 2.1 on page 8 and Figure 2.2 on page 9 shows an example ionosphere electron density profiles of day vs night. Another common phenomenon is a thin higher density of electrons forming called the sporatic E layer. Figure 2.3 on page 10 shows an example electron density profile of sporatic E layer formation. Typically sporatic E is a transient phenomenon occurring day or night. There is a some dependence on latitude with differences in formation between the equatorial and polar regions. Sporatic E is the one major exception to HF being the upper frequency limit of ionospheric reflection and cause VHF like FM radio to propagation far beyond the horizon. The causes of sporatic E are not well understood and not

predictable [3][13].

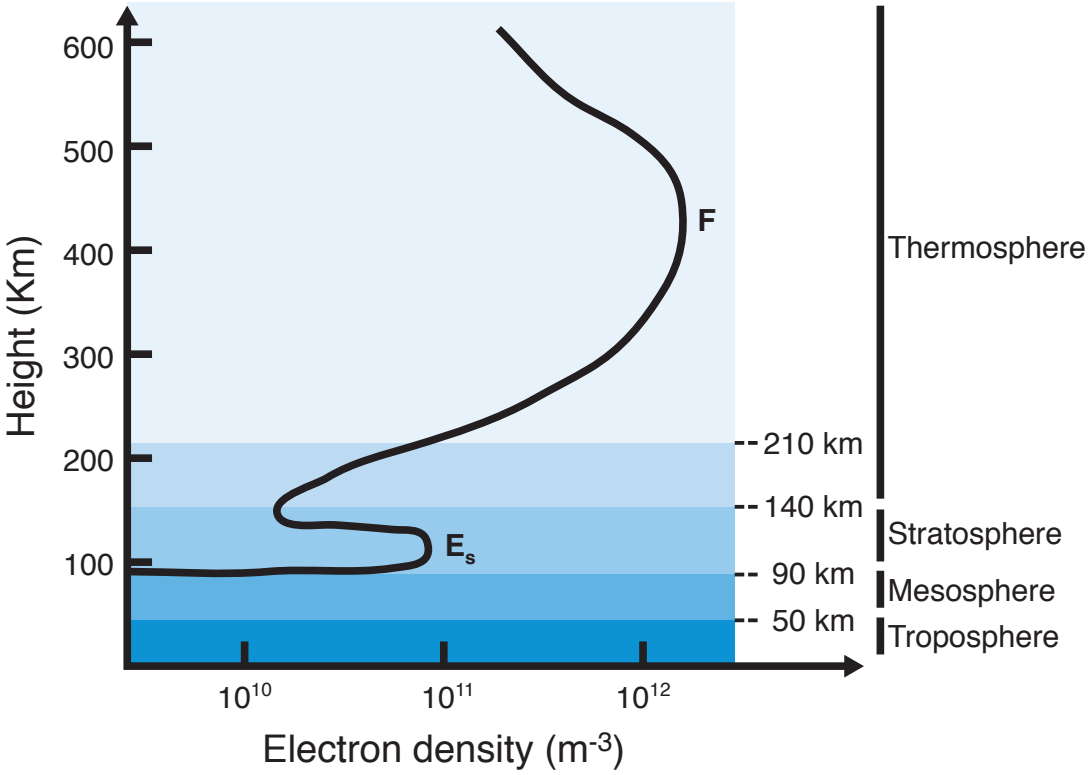

Figure 2.3: Ionosphere Sporadic E Layer

2.1.2 Ionosphere Movement

Because the ionosphere changes with the time of day and many other factors. This movement of the ionosphere causes spread in Doppler and range [3][4][13][14][15]. The ionosphere is a boiling soup of very low pressure atmosphere experiencing bombardment by ionizing radiation with localized pockets of higher density plasma. High altitude winds, storms, solar winds, solar storms, and local variation in chemistry all effects the rate of production and density of free electrons and there movement. Most applications that make use of the ionosphere are subject to the effects of dispersive

in both delay and Doppler. This Doppler spread is on the order of magnitude 1 Hz. The Doppler spread is caused by factors including high altitude air currents, storms, and changing time of day. Skywave communications and over the horizon radar are limited by this Doppler spreading. For OTHR this spreading widens the clutter ridge those reducing the ability for it to be suppressed and those reducing the ability targets with smaller Doppler shifts. Most of this kind of Doppler spreading can is difficult be suppressed or removed.

2.2 Ionosphere Material Properties

The ionosphere is composed varying density cold plasma . Because the ionosphere is a plasma the permittivity is a tensor with none zero of diagonal elements as expressed in Equations 2.1 a, b, and c. These off diagonal cause a polarization shift in a propagating Traverse Electromagnetic wave (TEM). The off diagonal elements of the tensor are imaginary and those give rise to two circular polarizations being the stable propagating modes. This takes the form of Right Hand Circularly Polarized (RHCP) and Left hand Circularly Polarized (LHCP). The right hand mode often referred to as the Ordinary or O mode propagates faster and with less attenuation then left hand mode often referred to as the X mode. Effective relative permittivity of the plasma is less than one. Equation 2.2 gives the effective permittivity as a function of the plasma frequency yet to be defined. The phase velocity of TEM wave in plasma is faster than that of free space as can be inferred from Equations 2.2 and 2.3. The group delay however is less then that of free space. This phase velocity being faster than that of air or free space causes total reflection when going beyond some critical

angle. [3][13][16][17][18][19][20]

$$\epsilon = \begin{bmatrix} \epsilon_{xx} & \epsilon_{xy} & 0 \\ \epsilon_{yx} & \epsilon_{yy} & 0 \\ 0 & 0 & \epsilon_{zz} \end{bmatrix} \tag{2.1a}$$

$$= \begin{bmatrix} \epsilon_x & -i\kappa & 0 \\ i\kappa & \epsilon_y & 0 \\ 0 & 0 & \epsilon_z \end{bmatrix} \tag{2.1b}$$

$$= \begin{bmatrix} 1 + \dfrac{{\omega_{pe}}^2}{{\omega_{ce}}^2 - \omega^2} & \dfrac{-i\omega_{ce}}{\omega}\dfrac{{\omega_{pe}}^2}{{\omega_{ce}}^2 - \omega^2} & 0 \\ \dfrac{i\omega_{ce}}{\omega}\dfrac{{\omega_{pe}}^2}{{\omega_{ce}}^2 - \omega^2} & 1 + \dfrac{{\omega_{pe}}^2}{{\omega_{ce}}^2 - \omega^2} & 0 \\ 0 & 0 & 1 + \dfrac{{\omega_{pe}}^2}{\omega^2} \end{bmatrix} \tag{2.1c}$$

$$\epsilon_{r\ plasma} = \left(1 - \frac{{f_p}^2}{f^2}\right) \tag{2.2}$$

$$\mathbf{C} = \frac{1}{\sqrt{\mu\epsilon}} \tag{2.3a}$$

$$= \frac{C_0}{\sqrt{\mu_r \epsilon_r}} \tag{2.3b}$$

$$= \frac{1}{\sqrt{\mu(\epsilon \pm \kappa)}} \tag{2.3c}$$

The driving factor for the electrical properties of the ionosphere is the electron density. Electron density N of a cold plasma is the driving factor of the plasma

frequency. The plasma frequency is the frequency where the propagation constant of the medium transitions from imaginary to real. Waves of a frequency above the plasma frequency are able to propagate. Below this frequency propagation of TEM waves are cut off. Equation 2.5 provides the relationship of the plasma frequency of the electron density. For Système international units this can be simplified and approximated to get equation 2.6. The impedance of the medium of the plasma expressed in Equation 2.8 derived from Equations 2.2 and 2.7. Note that below the plasma frequency the impedance is pure imaginary and propagation in the medium is not supported. Above the plasma frequency the impedance is real and does support propagation throw the medium. Table 2.1 shows example values for electron density and the approximate plasma frequencies for layers of the ionosphere. One factor conspicuously absent is the effect of the earths magnetic field on plasma. This is not needed to get an understanding of guiding of waves. Loss is also absent the discussion for frequencies above the plasma frequency. This is primarily caused by the interaction and collision of ions as the density is assumed to be low.

$$\beta_{\pm} = \omega\sqrt{\mu(\epsilon \pm \kappa)} \tag{2.4}$$

$$f_p = \frac{1}{2\pi}\sqrt{\frac{Ne^2}{m\epsilon_0}} \tag{2.5}$$

$$f_p \approx 9\sqrt{N} \tag{2.6}$$

Layer	Electron Density (m^{-1})	Plasma Frequency (MHz)
D Layer	10^{10}	0.10
E Layer Day	10^{11}	0.32
E Layer Night	10^{10}	0.10
F Layer Day	10^{13}	3.20
F Layer Night	10^{12}	1.00

Table 2.1: Example Plasma Frequencies of Ionosphere Layers

$$\eta = \sqrt{\frac{\mu}{\epsilon}} \tag{2.7a}$$

$$= \sqrt{\frac{\mu_0 \mu_r}{\epsilon_0 \epsilon_r}} \tag{2.7b}$$

$$= \eta_0 \sqrt{\frac{\mu_r}{\epsilon_r}} \tag{2.7c}$$

$$\eta_{\mathbf{p}} = \frac{\eta_0}{\sqrt{1 - \left(\frac{f_p}{f}\right)^2}} \tag{2.8}$$

2.3 Ionosphere Measurements

Ionospheric measurement methods leverage some of the factors described above. Each measurement method assumes a model of the ionosphere with some driving parameters. The simplest approximates the ionosphere as a thin dense layer of electrons. For some applications this is sufficient but says nothing about the structure of the ionosphere. Measurement exploits the changes of reflectivity as a function of altitude

and have the added benefit of having some structure of the ionosphere revealed by the nature of the measurement and model. Non of the measurements discussed here are capable of revealing the structure of the ionosphere and measure the top and bottom sides at the same time.

2.3.1 Ionosphere Sounders

Ionosphere sounders or ionosonde are upward looking radars measuring atmosphere reflectivity vs altitude. Ionosondes work by measuring the critical or plasma frequency verses altitude for vertical incidence. The critical frequency is the point when the impedance of the medium becomes real. Above the critical frequency the impedance of the medium is largely real and supports propagation. Below the critical frequency the impedance of the medium is largely imaginary and propagation is predominately attenuation. The circuital frequency is a function of the number of free electrons as described equation 2.5 and its approximation equation 2.6. Currently there are 5 ionosondes regularly operating in the United States.

2.3.2 GPS Total Electron Count

Total electron count or TEC measurements are an accumulation of electron density between two points of observation. These measurements are most commonly done with GPS signals. Figure 2.4 is an example GPS based TEC measurement provided by the National Oceanic and Atmospheric Administration (NOAA) [21]. This is done by comparing the time of arrival to the known distance to the satellite. Because of the frequencies used for GPS, propagation is very close to the free space path. The difference in time of arrival is accounted for by change in phase velocity in the atmosphere. Changing the value of ϵ in equation 2.3 on page 12 is used as the model accounting for the delay. Because of the near free space propagation and

measurement of accumulated path delay there is very limited information about the altitude structure of the ionosphere. The Klobuchar model ionosphere is a standard ionospheric correction for GPS and GNSS. This model approximates the ionosphere as a thin electron density layer at 350 KM. The Klobuchar model reduces Root Mean Square (RMS) errors caused by the by ionospheric destortion by as much as 50% [1].

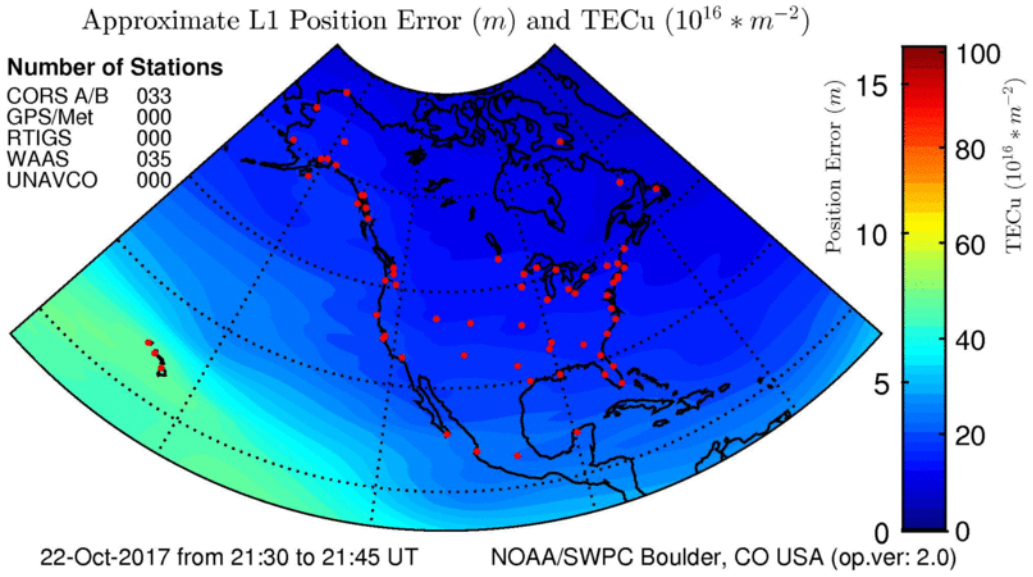

Figure 2.4: Example Total Electron Count Measurement for North America

2.3.3 Upper Ionosphere Measurements

There are currently two methods used for measurements of the top side of the ionosphere. Computing the difference between bottom side model and the TEC measurement described in section 2.3.2 and guessing the electron density profile. This method is not a measurement of structure and only yields the amount of electrons in the upper ionosphere. The Nequick ionospheric model makes use of this method[5]. Measurements of structure of the ionosphere require that ionosonde be placed in orbit. There are currently no such satellites in orbit, the last one was in 1975 as stated in Section 1.1.2. It is not practical to launch large numbers of ionosondes to obtain up

to date measurements of the ionosphere.

Chapter 3

IONOSPHERE CHANNEL MODEL

There are many methods of varying quality of modeling ionospheric channels. Ionospheric channel modeling is a complicated subject for all the reasons described in Chapter 2. The channel is dispersive in both delay and Doppler. Doppler dispersion for stationary transmitters and receivers is limited to less that 2 Hz[3]. Delay dispersion can be very large because of the long distances involved. This delay and Doppler dispersion is complicated by the fact the medium supports two propagating polarization modes O and X. The reasons for this are described in Section 2.2 starting on page 11. For frequencies that are well above the plasma frequency they are largely unaffected by the ionosphere other than the preference no right hand circularly polarized waves. The left hand circularly polarization propagates slower and is attenuated faster than the right hand polarization. For frequencies closer to the plasma frequency the effects are much stronger.

3.1 Layered Dielectric

The ionosphere being composed of progressive plasma density can be modeled as multiple layers of dielectric with discrete boundaries. These layers ruffly correspond to the D, E, and F layers and sub-layers of the ionosphere shown in Figures 2.1, 2.2, and 2.3. This is a common starting model for Over the Horizon Radars (OTHR) and HF skywave comunications [3][4]. The boundary of these layers can be modeled as desecrate transitions rather than a progressively changing dielectric. The reflection at the boundary is given by Equation 3.1 and the angles incidence and reflection are equation. Transmission at the boundary is given by Equation 3.2. The angle of

transmission follows Snell's law as shown in equations 3.4. The impedance at normal incidence is dictated by the plasma frequency from Equations 2.5 and 2.6 and can be calculated using Equation 2.8.

$$\mathbf{\Gamma} = \frac{\eta_1 - \eta_0}{\eta_1 + \eta_0} \tag{3.1}$$

$$\mathbf{T} = \frac{2\eta_1}{\eta_1 + \eta_0} \tag{3.2}$$

$$n = \frac{C_0}{\mathbf{C}} \tag{3.3a}$$

$$= \frac{C_0}{\beta} \tag{3.3b}$$

$$= \frac{C_0}{v} \tag{3.3c}$$

$$\frac{n_1}{sin(\theta_1)} = \frac{n_2}{sin(\theta_2)} \tag{3.4a}$$

$$\frac{\lambda_1}{sin(\theta_1)} = \frac{\lambda_2}{sin(\theta_2)} \tag{3.4b}$$

$$\tag{3.4c}$$

The approximation of the ionosphere as a stack of dielectric layers gives rise to the idea of maximum angle dependent on the frequency of operation. This is more useful articulated as the Maximum Usable Frequency (MUF). For low angles of α

higher frequency can be reflected and therefor propagate much longer that would normally be expected. The angle of total internal reflection at the boundary of two medium is given by Equation 3.5. Equations 3.5, 2.8, and 2.7 can be combined to get Equation 3.6 for the maximum useful frequency for a given angle. For ground to ground channels this is an approximate maximum frequency to get a desired reflection. For ground to space this is lower angle limit of rays that will make it to space.

$$sin(\alpha) = \sqrt{\frac{\epsilon_2}{\epsilon_1}} \tag{3.5}$$

$$f_{muf} = \frac{f_{plasma}}{sin(\alpha)} \tag{3.6}$$

3.2 Ray Tracing

Ray tracing extends the layered dielectric model described in Section 3.1 by removing the approximation of the discrete boundaries of between the layers of the ionosphere. The discrete boundary approximation is replaced with a continuous valve for electron density. All the equations described in Section 3.1 apply in their differential form. The differential form of Snell's law is shown in Equation 3.7. This is sufficient for a two dimensional ray tracer.

$$cot(\theta)d\theta = \frac{dn}{n} \tag{3.7}$$

Two dimensions is not sufficient to account for the structure of the ionosphere or the angular divergence of the O and X modes. Failure to account for the angular divergence can large errors because the interference pattern formed by the sum of the O and X modes. Accounting for this angular divergence and movement not contained

in the plane of propagation requires three dimensional ray tracing. The ray tracer used is PHARLAP and is described in Section 4.2.1 on page 27.

3.2.1 Ground to Ground

HF propagation for stationary ground to ground propagates in two methods surface wave and skywave. Surface wave works by a wave guided along the surface by virtue of the dielectric boundary of the surface of the earth and the air. This method is attenuated quickly at HF frequencies, however, it is the dominate method of propagation in lower frequencies. Skywave makes use of reflecting off of or being guided by the ionosphere. The simple version is a single reflection or bounce off of the ionosphere. Figure 3.1 illustrates this single reflection propagation. As described in two polarizations O and X propagate however the X mode is usual significantly attenuated when compared with the O mode. The propagation of both modes causes interference patterns at the receiver that are subject to the small movements of the ionosphere.

3.2.2 Ground to Space

Most ground to space scenarios involve at least one end not stationary with the exception of geosynchronous orbit. Frequency higher than the HF band is less effected by the properties of the ionosphere; However, polarization selectivity is still a major factor as the X mode is significantly more attenuated than the O mode. This is the reason for circular polarizations being preferred for satellite communications. Some bending or lenzing of the propagation path is present and more accurate models used for applications like GPS account for this [1][5]. Frequencies below the plasma frequency of the densest layer of the ionosphere do not propagate throw. This can be explained impedance of the medium becoming imaginary below the plasma frequency

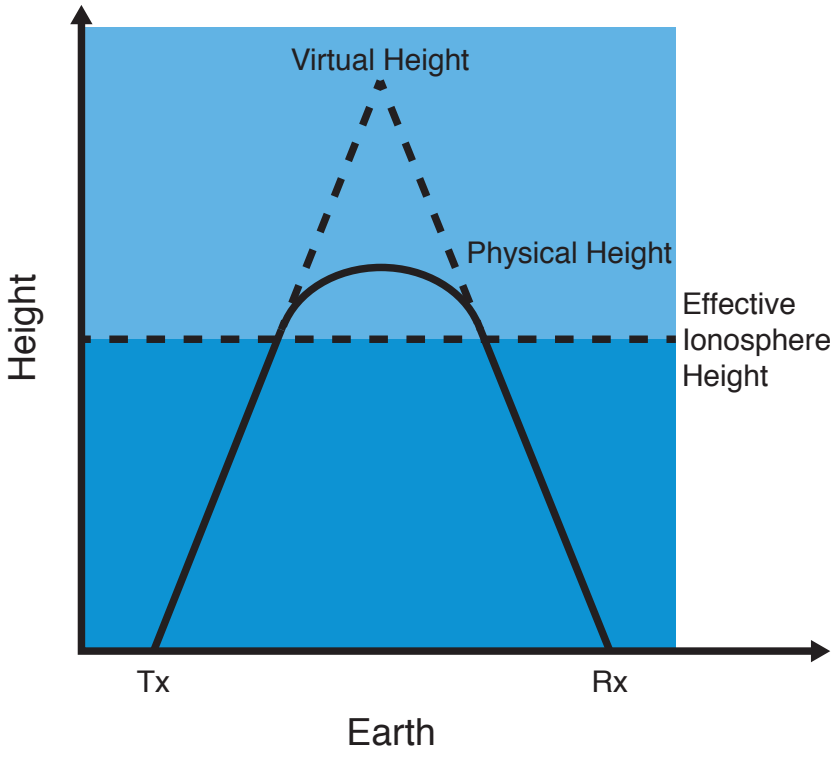

Figure 3.1: Ground to Ground Channel Utilizing the Ionosphere

as predicted by Equation 2.8. Frequencies in and around the HF band are strongly effected by the ionosphere while still propagating throw. Launch angles above the angle of maximum usage frequency will propagate into space or absorbed into to the ionosphere. The delay is much greater then that of the free space or geometric path length. This is because of the lenzing and bending of the propagation path. Doppler due to motion of the satellite is rate of change of the electrical path length between the ground emitter and the satellite. As mentioned before the path lengths are not that of the free space or geometric path length. This is not the only source of Doppler.

The ionosphere is continuously moving causing narrow band Doppler spread on the order of 1 Hz. Two polarization modes of propagation are supported and each has a unique path of propagation between the ground emitter and the satellite receiver. Because the paths are different they have differing delay and Doppler.

Chapter 4

EXPERIMENTS

No existing up to date regular measurements exist for electron density or structure of the top side of the ionosphere. Currently total electron count (TEC) using GPS signals are the only indirect observations of the upper ionosphere. For reasons discussed in 2.3.2 starting on page 15 little knowledge is revealed about the structure of the ionosphere from TEC measurements. Because of the frequency and type of measurement there is no revealed knowledge of the structure of the ionosphere and it's electron density. The combination of existing ionospheric sounders and GPS TEC measurement can be used to get total electrons above the highest observable altitude of the ionosphere. This is not sufficient for the purpose of understanding HF propagation in the upper ionosphere for reasons discussed in 2.2 starting on page 11.

The process of estimating the structure of the ionosphere starts with estimated parameters of the ionospheric channel. This is the channel between the fixed location ground emitter, through the ionosphere and to a satellite in orbit. Properties of propagation though the ionosphere are described in Section 2.2 and detailed specific to trans-ionospheric channels in Section 3.2.2. Estimating the ionospheric channel parameters are discussed in detail in section 5 starting on page 30. Any good estimate of the ionosphere structure should yield simulated channel parameters similar those observed from the measured data.

4.1 Satellite Experiments

Figure 4.1 illustrates the methodology used for converting the time evolution of a channel into to an estimate of the ionosphere. The process starts by estimating

some basic channel parameters including delay, Doppler and polarization of each mode. These are channel estimates and there evolution over time are compared with the guess of the ionosphere structure and the motion of the satellite. The process of updating the guess of the ionosphere is updated to minimize the error with the measured data. This kind of assimilation converges to a estimate of the ionosphere that has some relation with the true ionosphere structure. Unlike the measurement methods described in Section 2.3 this is affected by both the top and bottom sides and is sensitive to the structure of the ionosphere.

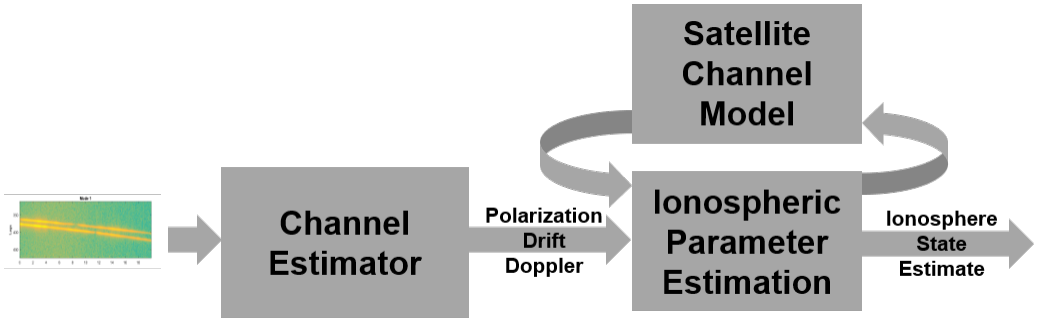

Figure 4.1: Block Diagram of Overall Processing System

4.1.1 Satellite and Instruments

The primary satellite used for these experiments has a crossed pair of dipoles connected to a two coherent channel receiver. Figure 4.2 is an illustration of the satellite used for measurements. Observe the pair large pair of crossed dipoles. Because of the wave lengths involved in the HF band these antennas are comparably large when compared with the satellite. The satellite in a polar orbit passes over known ground emitter. No specific information about the ephemeral of the satellite was given or details about the hardware united. The crossed pair of dipoles allow for observation of polarization incident to the satellite. Orientation is not known relative to the incident modes and therefore any observations of polarization measure is an known oblique

projection away from truth. The data provided from the satellite is matched filtered and in the form of complex range response verse time or fast time slow time.

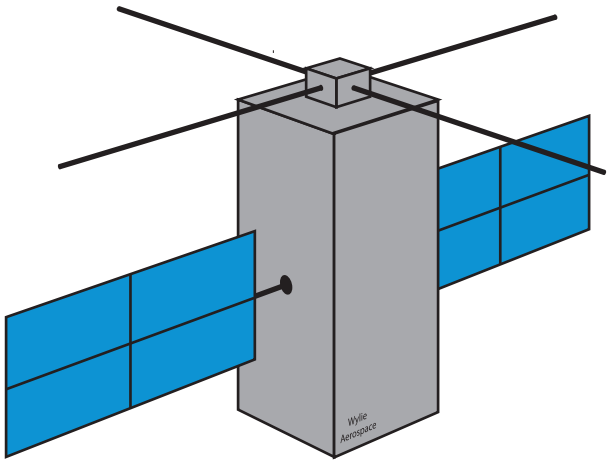

Figure 4.2: Illustration of the Satellite

4.2 Simulation

Simulation of the ionosphere is used both as a method of testing and directly in the estimation of the structure of the ionosphere. Simulation of the ionospheric propagation is using ray tracing using a software named PHARLAP described in detail in 4.2.1 The major difference between simulation and experiment is experiment is the starting point. Channel estimation using the methods outlined in Section 5 is the starting point of experiment. Simulation starts with selection of an ionosphere, gener-

ation of the delay and Doppler, generation of a simulated channel measurement using this delay and Doppler. The method of estimating the structure of the ionosphere is the same between simulation and experiments The end goal is the convergence of the ionospheric parameter estimator to an identical ionosphere.

4.2.1 PHARLAP

Ray tracing is used to simulate and predict the propagation in the ionosphere. PHARLAP is the ray tracer used. Written and maintained by Dr Manuel Cervera for the Australian government. PHARLAP is only a ray tracer. The software works using externally provided ionosphere model. By default the ionosphere model is IRI used by PHARLAP. Because of IRI's limited fidelity Boston College's ionospheric model RIPE is used. The reasons for this are discussed in Sections 4.2.2 and 4.2.3. Figure 4.3 shows an example 2D ray trace of an IRI ionosphere. Each white line represents a ray or a path of propagation. Observe the cut off distances for both ground to ground propagation and ground to space.

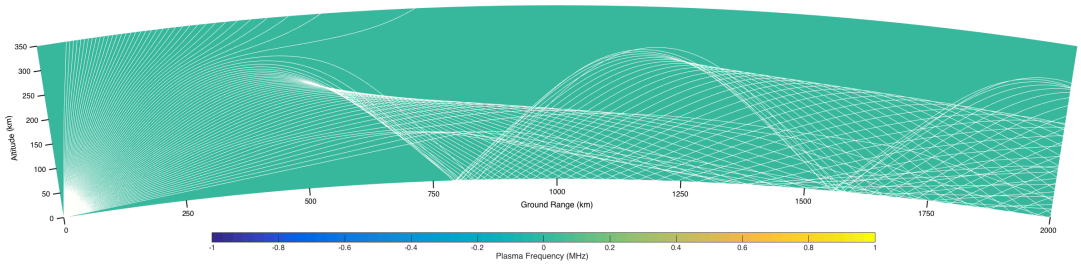

Figure 4.3: PHARLAP Example Ray Trace

4.2.2 International Reference Ionosphere

International Reference Ionosphere or IRI is an empirical climatological model of the ionosphere based on monthly average of the ionospheric sounder data and total electron count measurements [6]. Because of nature of the data used for the IRI

model, only bottom side of the ionosphere is observed. The top side of the ionosphere is scaled and adjusted to match TEC measurements. With no direct measurement of the top side and limited quality measurement of the middle of the ionosphere, these two regions of the ionosphere are poorly modeled. This is a starting point for the ray tracing based channel simulator. However, this is limited in the approximation that the ionosphere is static and smooth. The monthly averaging of the ionospheric sounders hides the time varying structure of the ionosphere. Depending on location and other factors the ionosphere is subject to changes on the order of minutes. Time of day, date, short term solar activity, and local variations are all effectively covered up or averaged away by IRI.

4.2.3 RIPE

RIPE is an improved ionosphere model driven by ionosonde data yielding a smooth three dimensional parametric model of the ionosphere. Developed by Boston College for the SHFT program. Currently RIPE makes use of data from 5 ionosondes around the United States. Because of the nature of the ionosphere and ionosonde only information of the bottom of the ionosphere drives the model. The upper structure of the ionosphere is assumed and scaled to match bottom side measurements. Ripe exposes a couple of parameters defining the top side electron density profile and scaling of the ionosphere. These parameters are the values adjusted in the optimization to match observations from the channel estimators.

4.2.4 Ionospheric Parameter Estimation

The method proposed to find the structure of the ionosphere is by adjusting the parameters of RIPE and simulating propagation using a PHARLAP ray trace simulation to match estimated channel parameters. This takes the form of a large and slow

optimization of adjusting the parameters of the ionospheric parameters exposed by RIPE minimizing the error with estimated channel parameters. Because of the very non-linear nature of the problem setup there is no guaranty of finding only a local minimum of error between the RIPE parameters and the observed channel parameters. Additionally, there is no external source of truth or validation of convergence to the true ionosphere. This last one is of less concern because a functionally accurate ionosphere is all that is needed.

Chapter 5

OVERVIEW OF CHANNEL ESTIMATION METHODS AND PROCESSING CHAIN

Over the course of this research many processing methods and techniques were applied to the problem of Ionospheric channel estimation. The definition of the problem has evolved over time with the type and availability of data and project direction. A data centric approach was taken when building parametric estimators of the ionospheric channel parameters. There was limited prior knowledge of the channel phenomenology for trans-ionospheric channels in the HF frequency band. Delay, Doppler, polarization, and polarization mode separation in delay and polarization are the final parameters are the final output parameters of the primary processing chain. Sections 5.1 to 5.7 starting on pages 31 to 39 covers the primary processing chain as shown in Figure 5.1. The results of these channel parameter estimates are used to drive the estimation of ionosphere parameters by means of ray trace based channel simulation.

The main channel estimation chain generates the estimates used as the end goal for the ionospheric estimator. The ionospheric estimator is discussed in Chapter 3 Section 4.2.4 starting on page 28. The input is range response sounding of the ionosphere over time, abbreviated r. This sounding includes polarization and is discussed in more detail in Section 4.1.1 starting on page 25. The outputs of the channel estimation scheme developed are delay, Doppler, polarization, and polarization mode separation for each of the respective polarization modes. Figure 5.1 is a block diagram overview of the channel estimation scheme developed as part of this work. The process starts with estimating and correcting for range migration of each of the respective modes

over a rolling window of the data. Sections 5.1 and 5.2 describe the drift estimation and correction in more detail. This is not the final estimate of drift or delay. However, this is sufficient for polarization estimation and parametric separation. Sections 5.3 and 5.4 describe the polarization estimation and parametric separation in more detail. The parametric separation allows each mode to be processed independently as the other modes have been removed or nulled. These parametrically isolated modes and the initial estimates for delay and drift are used for polynomial based estimates of delay/drift, and Doppler. The polynomial curve delay/drift and Doppler estimates impose continuity over a period of time. This polynomial delay/drift estimation is described in detail in Section 5.5. Doppler is estimated in a two stage process. Using the drift corrected data from the polynomial delay/drift estimate an initial Doppler estimate is used in computing using the periodogram. Using the initial Doppler as a starting point for the polynomial Doppler estimation, these two stages are detailed in Sections 5.6 and 5.5 respectively.

5.1 Windowed Drift Estimation

There is a problem of the satellite traveling across multiple range bins in a short period of time. This range bin migration is not because of the change in geometric or free space path, but due to the change in electrical path length. The Radon transform of the magnitude squared of range time data over a window of data is used to provide a course estimate of the drift. The major maxims correspond to the delays and drift of the respective propagating modes received. The number of major maxims is limited to two here corresponding to the plane wave propagation properties of the ionosphere supporting two distinct polarimetrically separate discribed in Section 3.1 starting on page 18.

This estimate of the delays and drift of each mode are passed to drift correction

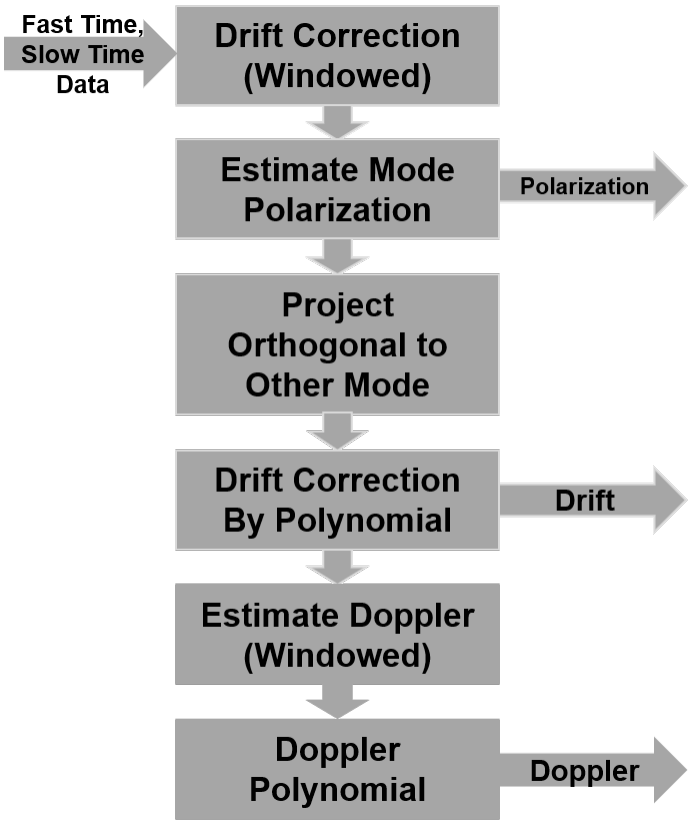

Figure 5.1: Block Diagram of Primary Processing Chain

block of the processing chain.

5.2 Drift Correction

Correcting for this range bin migration is done by using the estimates from section 5.1. The method used for re-sampling and shifting the range is based on the Discrete Fourier Transform (DFT) or Fast Fourier Transform (FFT). The shifting accounts for phase shifts of progression of the carrier. Equation 5.6d. In the absence of knowledge of the bandwidth or center frequency of the measurement Equation 5.7c is used. This complicates the Doppler Estimation process; however, polarization estimation process is uneffected by this unknown phase rotation. This is discussed in greater detail in Section 5.3 starting on page 35 on polarization estimation.

$$RB = \frac{\mathbf{C}}{BW} \tag{5.1}$$

$$f_c = \frac{\mathbf{C}}{\lambda} \tag{5.2}$$

$$\phi_{RB} = 2\pi \frac{RB}{\lambda} \tag{5.3}$$

$$BW_{frac} = \frac{BW}{f_c} \tag{5.4a}$$

$$= \frac{\mathbf{C}}{\overline{RB}} \tag{5.4b}$$

$$= \frac{\lambda}{RB} \tag{5.4c}$$

$$\phi_{RB} = \frac{2\pi}{BW_{frac}} \tag{5.5}$$

The derivation of delay shifting resampling method starts with the phase length of a range bin (RB). Equation 5.3 is the electrical phase of the carrier traversed by moving one range bin. The size of a range bin is dictated by the speed of light in the medium over bandwidth of the probing signal. Section 2.2 starting on page 11 details the speed of light in the medium using Equation 2.3. Reasonable values for the are tabulated in Table 2.1 on page 14. Using the free space of light is a reasonable approximation. Equation 5.4a is the definition of fractional bandwidth.

Substituting 5.1 solved for bandwidth and Equation 5.2 into the definition of the fractional bandwidth to get 5.4b. Simplifying 5.4b to get 5.4c. Rearranging 5.4c for RB and substituting into Equation 5.3 to get equation 5.5. Starting with the range response r shifting by the amount τ and rotating by the carrier phase due to the range migration τ to get Equation 5.6a. Applying the Fourier Transform properties to get 5.6b [22]. Substituting the Fourier Transform of the discrete delta into 5.6b to get Equation 5.6c. Equation 5.5 subsitued into 5.6c to get 5.6d. repeating the steps for Equation 5.6 with no information about carrier or bandwidth to get Equations 5.7a-c.

$$r_{shifted} = r * \delta(t-\tau) * e^{-i\tau\phi_{RB}} \tag{5.6a}$$

$$r_{shifted} = IFFT(\ FFT(r)\ FFT(\delta(t-\tau))\ e^{-i\tau\phi_{RB}}) \tag{5.6b}$$

$$r_{shifted} = IFFT(\ FFT(r)\ e^{-i2\pi\tau(-fft_{size}/2:fft_{size}/2)}\ e^{-i\tau\phi_{RB}}\ ) \tag{5.6c}$$

$$r_{shifted} = IFFT(\ FFT(r)\ e^{-i2\pi\tau(-fft_{size}/2:fft_{size}/2)}\ e^{-i\tau\frac{2\pi}{BW_{frac}}}\ ) \tag{5.6d}$$

$$r_{shifted} = r * \delta(t-\tau) \tag{5.7a}$$

$$r_{shifted} = IFFT(\ FFT(r)\ FFT(\delta(t-\tau))\ ) \tag{5.7b}$$

$$r_{shifted} = IFFT(\ FFT(r)\ e^{-i2\pi\tau(-fft_{size}/2:fft_{size}/2)}\ ) \tag{5.7c}$$

5.3 Polarization Estimation

Polarization estimates are used for separation of each polarization mode. No prior knowledge about the polarization is known or enforced. Using the delay and drift of each mode from Section 5.1 and the correction in Section 5.2 for the location and delay separation of each mode. The current polarization estimation works for 3 dimensional polarization measurement method; however, it is only tested with data from a crossed linearly polarized sampling data. This is discussed in greater detail in Section 4.1.1 starting on page 25. The end goal of the polarization estimate is to polarimetrically separate the two polarimetrically unique propagating modes, O and X, of the ionosphere. This polarimetric selection is illustrated in Figure 5.2 Modes A and B are used for surrogates of the O and X modes because of the absence spacial orientation knowledge.

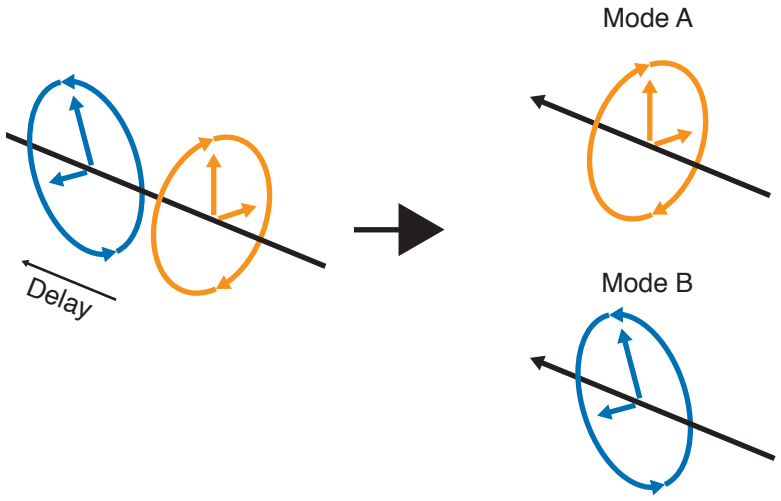

Figure 5.2: Polarization Separation

The method to estimate the polarization is that of estimating the projection of

the incident polarization onto the receive antenna element. Maximizing the inner product range amplitude response (r) and the auto-correlation R) of the transmitted waveform shifted by τ. This maximum inner product for each respective mode is the estimate of the projection of that mode i onto the antenna sampling or $p_{ppa\ i}$. Equation 5.8 shows this maximization around the corresponding delay for the respective mode. Repeating this process for every mode of the m desired modes and n antenna samplings combinations. Each of these estimates form the estimate of the projection of each polarization onto the receiving antenna array. The vector of the estimates of each polarization mode is normalized to unit magnitude to form the estimate of the incident polarization or $\vec{p_{ppa}}$. Equations 5.9 and 5.10 show the method to arrive at the polarization vector estimate. In the absence of information about the auto correlation of the waveform used a *sinc* is used. The *sinc* is scaled in accordance with bandwidth knowledge shown in Equation 5.11.

$$p_{ppa\ i} = max_{\tau}(r_i \cdot R(\tau)) \tag{5.8}$$

$$\vec{p_{ppa}} = \begin{bmatrix} p_{ppa\ 1} \\ p_{ppa\ 2} \\ \\ \\ p_{ppa\ n} \end{bmatrix} \tag{5.9}$$

$$\vec{p_{ppa}} = \frac{\vec{p_{ppa}}}{\vec{p_{ppa}}^{\dagger}\vec{p_{ppa}}} \tag{5.10}$$

$$R(t,\tau) = sinc\Big(\frac{t-\tau}{BW}\Big) \tag{5.11a}$$

$$= \frac{sin(t-\tau)}{t\ BW} \tag{5.11b}$$

5.4 Orthogonal Polarization Projection

The selection of a single polarization mode is done by projecting orthogonal to the undesired polarization. Equation 5.12 is the estimate matrix formed from the method described in Section 5.3. This is done by computing the null space of polarization estimate matrix in Equation 5.12 less the desired polarization estimate of the desired mode and projecting the original data onto the new basis. This linear polarization sampling to arbitrary polarization transform is illustrated in Figure 5.3.

$$P_{ppa} = \left[\vec{p_{ppa}}_{1} \quad \vec{p_{ppa}}_{2} \quad \dots \quad \vec{p_{ppa}}_{m} \right] \tag{5.12}$$

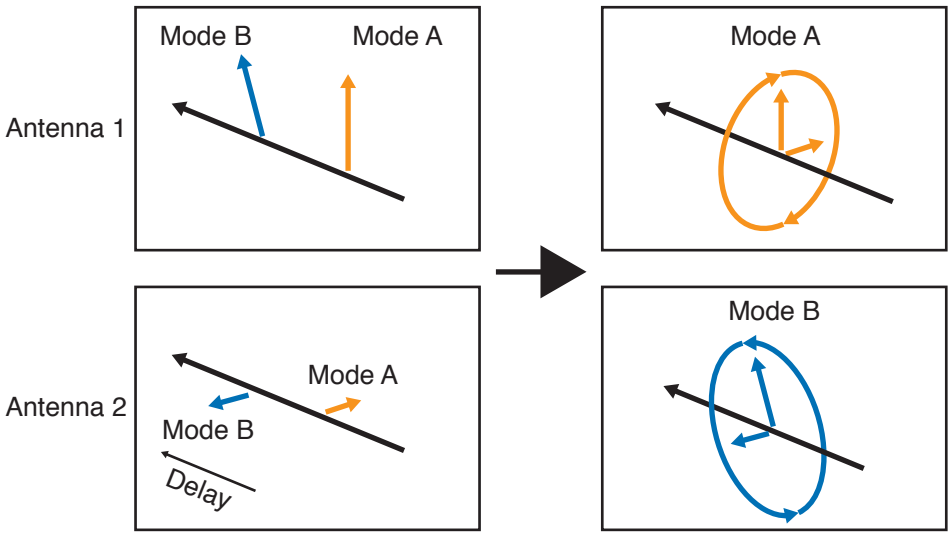

Figure 5.3: Linear to Arbitrary Polarization Selection

5.5 Polynomial Drift Estimation

Polynomial Drift estimation starts with the polarimetrically separated data computed in Section 5.4 and the initial delay/drift estimates computed in section 5.1. This polarimetrically separated data is the original data set projected onto the estimated basis that nulls the other modes as described 5.4. Equation 5.13 describes the formulation of the polynomials used. Initial guesses of the polynomial are computed using MATLAB's polyval function. Order selection is a subject of hand tuning at this point. Maximizing the fit function described in Equations 5.14 a and b over time T_1 to T_2 to yields the estimate the polynomial coefficients. This is easily transformable into delay estimates by evaluating the polynomial for the desired time.

$$d_p(t) = \sum_{j=0}^{n} d_j t^j \tag{5.13a}$$

$$= d_n t^n + \cdots + d_2 t^2 + d_1 t + d_0 \tag{5.13b}$$

$$fit(d_1 \ldots d_n) = \sum_{t=T_1}^{T_2} \Big(|RTI[d_p(t), t]|^2 \Big) \tag{5.14a}$$

$$= \sum_{t=T_1}^{T_2} \Big(|RTI[:, t] - RTI[d_p(t), t]|^2 \Big) \tag{5.14b}$$

$$max_{d_1 \ldots d_n} \Big(||fit(d_1 \ldots d_n)|| \Big) \rightarrow \hat{d}_p \tag{5.15}$$

5.6 Windowed Doppler Estimation

Doppler estimation over a small window is a standard spectral estimation problem. This is done with polarimtrically separated data drift corrected using polynomial drift

estimate from Section 5.5 above. Because the windowed Doppler estimated is only used as initial condition for the polynomial Doppler estimator it only needs to be close enough for the optimization used in to converge to the correct value. The periodogram over a sliding window is used to estimate the Doppler. The size of the window and how often it is computed is the subject of some hand tuning. With information about the carrier and bandwidth of this Doppler estimate is the deviation from the Doppler caused by rate of change in the electrical path length. The absence of information about the carrier and bandwidth this estimate is the Doppler shift estimate.

5.7 Polynomial Doppler Estimation

The polynomial method for estimating Doppler follows the polynomial delay/drift method outlined in section 5.5. The difference is the polynomial is the an expression of the phase of the carrier. This is reflected in the difference between Equations 5.13 and 5.16. Two versions of the fit function are constructed. Equation 5.17a is weighted to higher SNR conditions of the data set. Equation 5.17b is weighted and tries to imposes continuos phase across the RTI.

$$Dop_p(t) = e^{i2\pi\sum_{j=0}^{n} d_j t^j} \tag{5.16a}$$

$$= e^{i2\pi d_n t^n + \cdots + d_2 t^2 + d_1 t + d_0} \tag{5.16b}$$

$$= e^{i2\pi d_n t^n} \ \ldots \ e^{i2\pi d_2 t^2} \ e^{i2\pi d_0 t} \tag{5.16c}$$

$$fit(d_1 \dots d_n) = \Big| \sum_{t=T_1}^{T_2} \Big(RTI[d_p(t), t] \; Dop_p^{\dagger}(t) \Big) \Big| \tag{5.17a}$$

$$= \Big| \sum_{t=T_1}^{T_2} \Big(\frac{RTI[d_p(t), t]}{|RTI[d_p(t), t]|} \; Dop_p^{\dagger}(t) \Big) \Big| \tag{5.17b}$$

$$max_{d_1 \dots Dop_n} \Big(||fit(Dop_1 \dots Dop_n)|| \Big) \rightarrow \hat{Dop}_p \tag{5.18}$$

5.8 Angle of Arrival

Angle of arrival methods offer additional degrees of measurement of the channel between the ground emitter and the satellite receiver. The polarization estimator described in Section 5.3 can be used for angle of arrival when a complete spacial sampling is used with complete three dimensional polarization measurements. This requires at least three crossed dipoles to properly observe any possible incident polarization vector. Multiple in band ground emitter offer the ability to observe multiple highly correlated channels between the ground emitters and the satellite. This is done by frequency shifting each emitter by more then the physical Doppler of the system. A couple of methods of angle of arrival explored and implemented; however, none of them where tested with data.

Chapter 6

RESULTS

A limited sample of real data was provided with little information about about the measurement setup. This was a range amplitude verses time about 20 seconds long with no information about the range, location, time, or waveform being observed. The data is provided already matched filtered. Because no information is given about the waveform a least squares estimates are not possible. The delay/drift estimation results and considerations are detailed in Section 6.1 below.

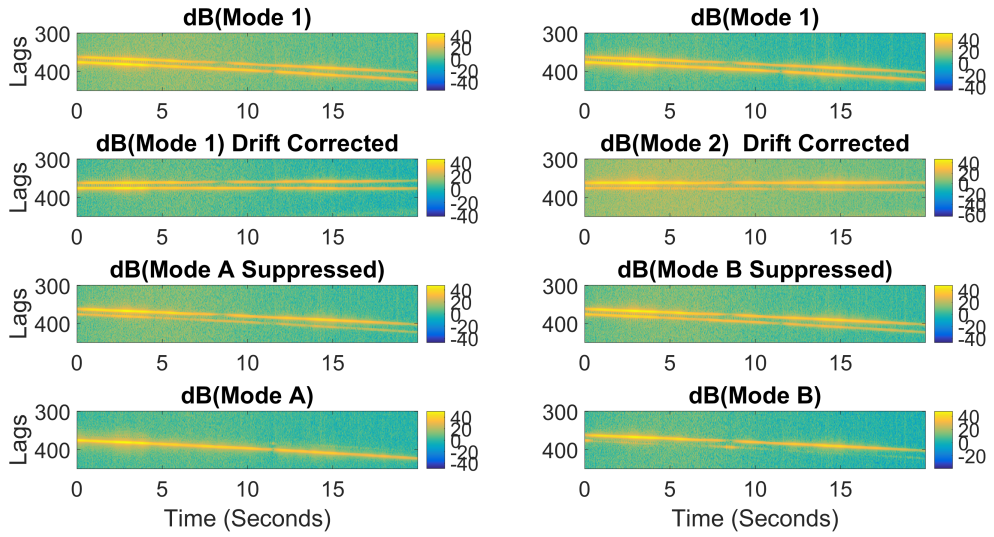

Figure 6.1: Over of Processed Data

6.1 Drift Estimation and Correction

The delay/drift estimate of the data described in Sections 5.1 and 5.5 used to produce estimates of the delay and its evolution over time. No performance metric of the of the polynomial estimator was dirived or Because of the limited

6.2 Polarization Separation

Ideally the polarimetric separation of the O and X modes should be perfect as RHCP and LHCP are orthogonal. Figure 6.2 shows the inner product of the polarization estimates for modes A and B. Figure 6.2 shows the inner product of the unit magnitude polarization estimates evolution with time and the respective energies of each mode. They appear to be not well separated as the inner product is only about -5 dB. There are a couple of factors causing this. The satellite has some unknown rotation and rotation rate to the incident field. This rotation causes an oblique projection of the polarization vector onto the observing antenna array reducing the separation of modes. The oblique projection is partially why the two observed polarization modes are referred to as A and B and not O and X.

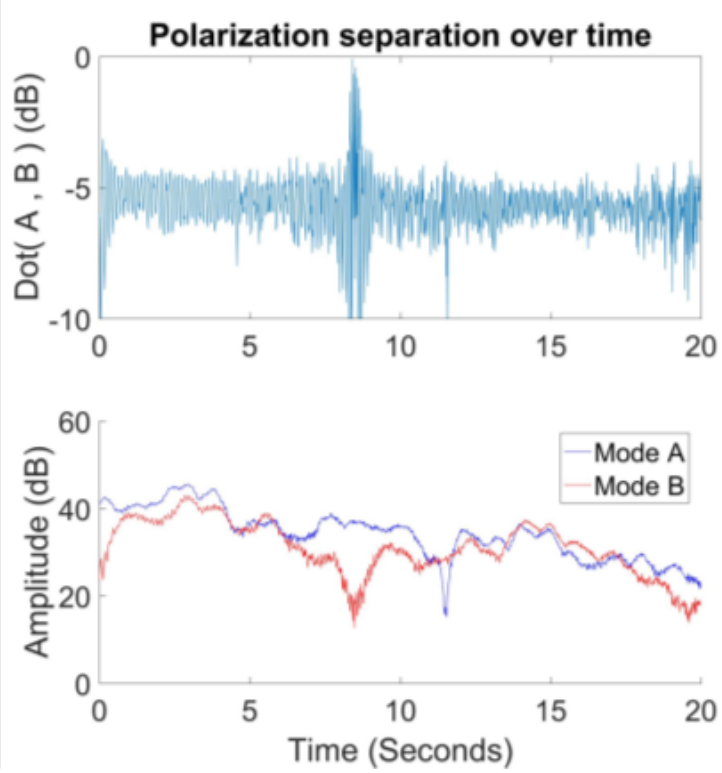

Figure 6.2: Polarimetric Separation of Modes

The signal to noise ratio (SNR) of each mode has a strong impact on the quality of

the polarization estimate and the ability to project orthogonal projection using this estimation. Because at some points in the provided data set both modes A and B are reduced in SNR and therefore reduces the quality of the polarization estimates. The effects of this can be seen around 8 seconds in Figure 6.2 when mode B fades for a short period of time causing the separation of the polarization estimate of mode B to become that of the back ground energy and the corresponding delay. The impulse of response of the channel of each polarimetrically separate mode can be seen in Figure 6.3. This impulse response is delay shifted using the windowed delay/drift estimate described in Section 5.1. The visible leakage of mode A into mode B matches with the low SNR of mode B about 8 seconds into the data set. The appearance of some kind of period structure in the inner product of the polarization estimates in Figure 6.2 is yet unexplained and could be caused by many factors beyond the scope of this document.

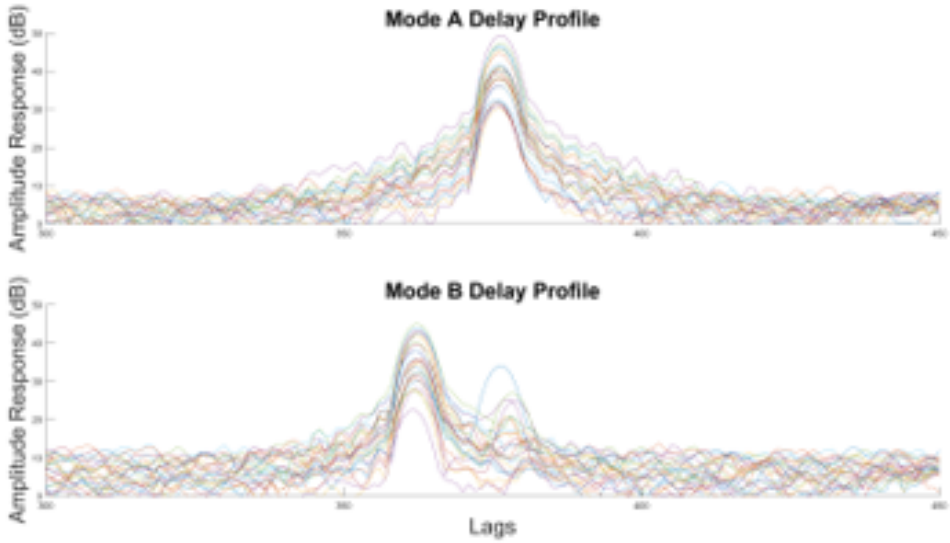

Figure 6.3: Single Mode Impulse Response

6.3 Doppler Estimation

Because of the Data provided the Doppler estimates are not meaningful. Doppler is a function of the center frequency and the relative motion of the platform. The width of viable Doppler resolution is limited between half to sample rate below and half to sample rate above the carrier. They are subject to multiple Nyquist aliasing those reducing the useful of the data. Additionally, this aliasing causes the Polynomial estimates of phase and Doppler to not converge to a usable answer. With information about the frequency of the carrier and the bandwidth of the transmitted signal the Doppler due to change electrical path length is estimated using the polynomial delay/drift estimation because of the drift correction method described in Section 5.2. The Doppler estimated is using the Doppler estimation tools outlined in Sections 5.6 and 5.7 is the deviations from electrical path length model. The causes for these deviations include clock and frequency offsets of the transmitter and the receiver as well as local ionospheric proporties and movement described in Sections 2.1 and 2.1.2.

6.4 Methods in the Absence of Data

Many of the processing methods considered where not able to be tested because of a lack of data and problem definition. These are mostly the angle of arrival methods. Time and frequency of arrival angle estimates where written; however, because of the changing scope of the problem they where not useful in there original form. Versions of time and frequency of location arose from PHARLAP simulation that more closely resemble back projection.

Chapter 7

FUTURE WORK

7.1 Estimators

Measure of performance is needed evaluate the quality of an estimator. Currently nothing like a Cramer-Rao bound or other performance metric exists for any of the polynomial based delay/drift and Doppler estimators described in Chapter 5. This exists for the windowed Doppler estimates and delay/drift with some assumptions about the nature of channel that may not hold true [4][14][23]. The polarization estimation method is a linear estimator technique that a Cramer-Rao bound can be found. Some of these assumptions are backed up by the physics of propagation in the ionosphere described in Chapter 2. This is because of the single frequency assumption of the ionospheric model. Over a small bandwidth this is sufficient; however, little significant study has been given to the effects of bandwidth. Currently the absence of information about the waveform means a least squares estimate of the channel can not reasonably be obtained. Because of this, both leakage of the O and X modes into each other and waveform auto-correlation these estimators cause the estimators have some bias. Additionally, the absence information about the carrier and the bandwidth used meaningful Doppler estimates can not be obtained from the data provided. This is discussed in Sections 5.6 and 5.7 as well as Section 6.3 in more detail.

7.2 Improved Initial Guess of the Ionosphere

Currently GPS TEC measurements of the ionosphere are an indirect method of obtaining sum using an initial guess about the top side structure of the ionosphere.

This is due in large part to the propagation of the ionosphere at the frequencies used by GPS and the very simplified models, like Klobuchar, of the ionosphere that can be used [1]. This is described in greater detail in Chapter 2 and discuses in detail in Section 2.3.2. Currently only the 5 ionosondes located around the United States are integrated into the RIPE ionosphere model. No factors like differences in time of arrival the ordinary and extraordinary polarization, polarization and plain of incidence, or dispersion with in a single mode are unitized to gain additional information about the ionosphere. This may be the information found be the parameter estimation method outlined in Chapter 2 and discuses in detail in Section 4.2.4. It may aid with a better initial guess, converge faster and to the more appropriate fit of the ionosphere.

7.3 External Validation

There are currently no downward looking ionosondes in orbit observing or other method of observation the top side of the ionosphere no external validation of the estimated ionosphere is possible. The last of these ionosondes was in 1975 with the AEROS B satellite. GPS based TEC measurements make use of an effective total electron count and assumed that is not necessarily pertinent. The method of estimating the ionosphere outlined in Section 4.2.4 can fall into local minimum yielding a very close channel response for the specific satellite pass but may have limited predictive properties. Some of the methods hinted at in Section 7.2 may reduce the potential to convergence on local minimums that are not representative of the ionosphere. A second observation satellite like what was used for the channel measurements could provide some validation and fidelity however would not solve the problem of no external validation.

7.4 Data with Direction of Arrival and Polarization

No measurement data that could make use of angle or arrival or gives complete polarization information has been made available. There are a couple of reasons including program time-line and equipment malfunction. Some data with polarimetric observation where provided; however, because of means of observation described in Section 4.1.1, 5.3, and 6.2 could not be fully unitized. This is because of the satellite only has a pair of crossed dipoles and therefore is blind to polarization not contained in the plane of the dipoles. Angle of arrival of multiple concurrent ground emitters could improve the estimation of the ionosphere structure by multiple concurrent observations of specially close channels. This can be done by prepossessing of the data to form multiple interdependent range response verse time measurements.

Chapter 8

SUMMARY

The study of radio propagation involving the ionosphere is almost as old as radio. Most of the study has been focused on ground to ground propagation not ground to space. Only studying ground to ground no measurements of the upper ionosphere where possible until the advent of satellites. Satellites enabled limited measurement of the upper ionosphere using the same methods when observing the lower ionosphere. Some study of space to ground channels using GPS has been done and is not sensitive to the details of the ionosphere because of the frequencies used. The structure of the ionosphere is not static, regular observations are required. Multiple models of the ionosphere exist of varying fidelity using the aforementioned properties. Most of the models are do not represent the time evolution of the ionosphere. Because of this Boston College developed RIPE an assimilation based model of the ionosphere using existing ionosondes. This is outlined in chapters 1, 2, and 3 respectively.

The model of the ionospheric channel model properties outlined in chapters 2 and 3 describe some important parameters driving the model. Estimating these parameters is the focus of chapters 4, 5, and 6. Polarimetric separation of the two propagation paths yields improved estimates of the important parameters of the model. Correcting for range migration using incoherent processing of the data yields a good initial estimates of delay and Doppler. These initial estimates are used as initial conditions to form delay and Doppler estimate fit using polynomial curves. Angle of arrival was explored and simulated but because of a deficiency of data not experimentally tested.

The estimated parameters are sufficient observation of the ionosphere.

8.1 Conclusion

The goals of this work where to develop a channel model for ground to space propagation throw the ionosphere and the tools estimate from the data the channel. The proposed model is comprised two unique polarization that propagation at different velocities and paths caused by the properties of magnetized cold plasma that is the ionosphere. The mechanism for this polarimetric separation of paths is derived and backed up by simulation using PHARLAP ray tracing. Tools to estimate and separate based on polarization are outlined, defined, and shown to work. Using this polarimetric separation the respective delay and Doppler can be estimated using polynomial fit functions. The combined methods yield meaningful estimates of the parameters of the ionospheric channel model outlined and enable study of the ionosphere structure and properties at all altitudes.

REFERENCES

[1] J. A. Klobuchar, "Ionospheric time-delay algorithm for single-frequency gps users," *IEEE Transactions on Aerospace and Electronic Systems*, vol. AES-23, no. 3, pp. 325–331, May 1987.

[2] M. B. El-Arini, W. Poor, R. Lejeune, R. Conker, J. Fernow, and K. Markin, "An introduction to wide area augmentation system and its predicted performance," *Radio Science*, vol. 36, no. 5, pp. 1233–1240, Sept 2001.

[3] G. Fabrizio, *High frequency over-the-horizon radar : fundamental principles, signal processing, and practical applications.* New York: McGraw-Hill Education, 2013.

[4] M. Richards, W. Holm, and J. Scheer, *Principles of Modern Radar: Basic Principles*, ser. Electromagnetics and Radar. Institution of Engineering and Technology, 2010.

[5] S. Radicella and B. Nava, "Nequick model: Origin and evolution," pp. 422–425, 11 2010.

[6] "International reference ionosphere." [Online]. Available: https://iri.gsfc.nasa.gov/

[7] L. Scherliess, D. C. Thompson, and R. W. Schunk, "Ionospheric dynamics and drivers obtained from a physics-based data assimilation model," *Radio Science*, vol. 44, no. 01, pp. 1–8, Feb 2009.

[8] I. Galkin, X. Huang, B. Reinisch, A. M. Vesnin, D. Bilitza, S. Fridman, M. Pezzopane, B. Zolesi, and C. Scotto, "Assimilation of sparse continuous groundbased ionosonde data into iri using nectar model morphing," pp. 1–1, 05 2015.

[9] P. A. Bernhardt, M. A. Hei, C. L. Siefring, and M. R. Wilkens, "Predictions of hf system performance for propagation through disturbed ionospheres measured using low-earth-orbit satellite radio beacon tomography," *Radio Science*, vol. 49, no. 7, pp. 506–517, July 2014.

[10] L. Scherliess, R. W. Schunk, J. J. Sojka, and D. C. Thompson, "Development of a physics-based reduced state kalman filter for the ionosphere," *Radio Science*, vol. 39, no. 1, pp. 1–12, Feb 2004.

[11] I. Galkin, B. Reinisch, X. Huang, and D. Bilitza, "Assimilation of giro data into a real-time iri," vol. 47, 04 2012.

[12] P. Cosson, B. Nava, and S. Radicella, "On the use of nequick topside option in iri-2007," *Advances in Space Research*, vol. 43, no. 11, pp. 1688 – 1693, 2009, ionosphere - Modelling, Forecasting, and Telecommunications I.

[13] R. W. Schunk, *Ionospheres : physics, plasma physics, and chemistry.* Cambridge, UK New York: Cambridge University Press, 2009.

[14] M. A. Richards, *Fundamentals of radar signal processing.* New York: McGraw-Hill Education, 2014.

[15] J. A. Jacobs and T. Watanabe, "Doppler frequency changes in radio waves propagating through a moving ionosphere," *Radio Science*, vol. 1, no. 3, pp. 257–264, March 1966.

[16] R. Dendy, *Plasma Dynamics*, ser. Oxford science publications. Clarendon Press, 1990.

[17] J. R. Wait, *Electromagnetic Waves in Stratified Media (Ieee/Oup Series on Electromagnetic Wave Theory).* Ieee, 1995.

[18] D. K. Cheng, *Field and Wave Electromagnetics (2nd Edition).* Addison-Wesley, 1989.

[19] P. C. Clemmow, "The theory of electromagnetic waves in a simple anisotropic medium," *Electrical Engineers, Proceedings of the Institution of*, vol. 110, no. 1, pp. 101–106, January 1963.

[20] D. M. Pozar, *Microwave Engineering.* Hoboken, New Jersey: John Wiley & Sons, 2005.

[21] "North american total electron content." [Online]. Available: http://www.swpc.noaa.gov/products/north-american-total-electron-content-us-region

[22] D. W. Bliss and S. Govindasamy, *Adaptive Wireless Communications: MIMO Channels and Networks.* Cambridge University Press, 2013.

[23] S. Kay, *Fundamentals of Statistical Signal Processing: Estimation theory*, ser. Fundamentals of Statistical Signal Processing. PTR Prentice-Hall, 1993.

BIOGRAPHICAL SKETCH

Wylie Standage-Beier is currently a masters degree at Arizona State University in Electrical Engineering with focus of Signal Processing. In the Fall 2017 he will graduate with a his masters and continue to pursue a PHD in the same field of study. He graduated with his under graduate degree in the fall of 2014 in Electrical Engineering from Arizona State University.